Zhao *et al.*
European Journal of Medical Research (2025) 30:1116
https://doi.org/10.1186/s40001-025-03278-9

European Journal of Medical Research

RESEARCH

Open Access

Ultrasound super-resolution microvascular imaging of kidney microvascular alterations in acute kidney injury on a clinical ultrasound scanner

Ping Zhao[1,2,3†], Jianing Zhu[2†], Huina An[2], Luda Song[2], Yiru Wang[2], Qiuyang Li[2*] and Yukun Luo[1,2,3*]

Abstract

Background Early assessment of acute kidney injury (AKI) is critical to the prognosis of patients. Kidney microcirculation hemodynamic changes are pivotal to AKI pathogenesis. This study aims to evaluate the feasibility of ultrasound resolution microvascular (URM) imaging in evaluating kidney microvascular alterations in ischemia–reperfusion induced AKI using a clinical ultrasound scanner, with qualitative and quantitative microvascular analysis.

Methods Sprague Dawley rats were randomly divided into ischemia–reperfusion injury (IRI), sham and control groups. Kidney microvascular characteristics were captured using URM. URM images were compared with color Doppler and superb microvascular imaging (SMI). In addition, URM was capable of providing quantitative information on blood density and velocities. After ultrasound examination, kidney tissues were fixed for pathological sectioning and examination.

Results Compared to color Doppler and SMI techniques, interlobar, arcuate, cortical radial vessels, and part of the medullary organization were more visible on URM density maps. URM identified vessels 4–7 times thinner compared with color Doppler and SMI. The average URM smallest analyzable vessel was 0.11 ± 0.01 mm. Furthermore, quantitative findings demonstrated significant differences in kidney cortical mean vessel ratio, mean density and perfusion index between the IRI group and both control and sham groups ($p < 0.0001, = 0.0237, = 0.0028$). These parameters correlated significantly with CD31 immunohistochemistry ($r = 0.62–0.68$).

Conclusions This study demonstrates the feasibility of URM in AKI using a conventional clinical ultrasound scanner, with simple examination procedure and post-processing tools. Hence, this technique could be a promising diagnostic tool for qualitative and quantitative kidney microvascular assessment.

Keywords Ultrasonography, Ultrasound super-resolution microvascular, Microvascular density, Ischemia–reperfusion injury, Acute kidney injury

†Ping Zhao and Jianing Zhu have contributed equally as co-first author.

*Correspondence:
Qiuyang Li
liqiuyang0925@163.com
Yukun Luo
luoyukun@301hospital.com.cn
Full list of author information is available at the end of the article

Introduction

Acute kidney injury (AKI) is a severe clinical condition characterized by a rapid decline in kidney function. This condition leads to significant morbidity and mortality, necessitating the development of advanced diagnostic tools for early detection and monitoring [1]. The kidney microvasculature plays a crucial role in the pathophysiology of AKI, with microvascular alterations such as congestion, rarefaction, and endothelial dysfunction contributing to the progression of kidney damage [2, 3].

Existing noninvasive imaging methods for quantifying kidney microvascular alterations are still lacking. Micro-computed tomography (micro-CT) [4] and magnetic resonance imaging (MRI) [5] have been successfully used in preclinical studies for imaging the changes in kidney microvascular structures. They all offer only indirect assessments, lacking the ability to directly visualize the microvasculature. Although these imaging methods achieve high spatial resolution, they each have their limitations. Micro-CT is limited by harmful radiation and the constraints of contrast agents. As for MRI, the imaging systems are bulky and costly, which hinders their widespread or repeated application. Ultrasound, with its inherent benefits of safety, noninvasiveness, portability, cost-effectiveness, and user-friendliness, has seen various techniques explored, including Doppler imaging and contrast-enhanced ultrasound (CEUS), both in animal models and clinical settings [6–8]. However, due to the limitations imposed by acoustic diffraction, these methods have not achieved the high spatial resolution necessary for the assessment of microvasculature. Therefore, there is a pressing need for imaging techniques that can provide high-resolution, noninvasive assessment of kidney microvasculature.

Ultrasound resolution microvascular imaging (URM) has emerged as a promising technology capable of overcoming the resolution limits of conventional ultrasound [9]. By utilizing microbubble contrast agents and advanced signal processing techniques, URM can achieve spatial resolutions down to the micron level, enabling detailed visualization of microvascular structures. In previous studies, URM has successfully applied for in vivo microvascular imaging in mouse brain [10], mouse kidney [11], and human organs [12, 13]. However, these studies required research on the ultrafast ultrasound scanners, which are not commonly available in clinical settings, and involve lengthy acquisition times. Furthermore, the signal processing procedure following ultrasound data acquisition is implemented offline, lacking the capability for real-time analysis.

This study aims to explore the feasibility of URM in assessing kidney microvascular changes in a rat model of kidney ischemia reperfusion injury (IRI) using a clinical ultrasound scanner. The imaging system was not modified, and post-processing steps were performed directly on the segments recorded by the scanner. Therefore, this technique is easy to replicate without the need to develop new hardware. In this study, we describe the imaging protocols and post-processing steps required to perform URM. In addition, we quantitatively assessed the kidneys for changes in vessel density, perfusion index and vessel velocity, based on the URM kidney images. The results from URM assessment on vessel density were correlated with histological analysis as a gold standard for validation.

Materials and methods

Animal experiments

Eighteen male Sprague Dawley rats (300–330g) were allowed to acclimatize for 1 week before experiments. All rats were housed in a temperature-controlled room (22 ± 1 °C) with a 12 h light–dark cycle and had free access to food and water. The animals were provided by the hospital. The study protocol was approved by the Ethics Committee of the hospital (2023-X19-45).

Rats were fasted with access only to water for 24 h and weighed. Then rats were randomly divided into an IRI group ($n=6$), sham group ($n=6$) and a control group ($n=6$). Anesthesia was induced with 5% isoflurane in 65% nitrogen and 35% oxygen; 1–2% isoflurane maintained the anesthesia. The hair at the bilateral kidney area was removed, and the skin was exposed before surgical process. The IRI group was as follows: a 1.5–2 cm incision was made on the bilateral lateral abdomen, and the lateral abdominal opening, the renal hilum was separated, and the renal arteries and veins were clamped using atraumatic vascular clamps for 45 min. Restoration of renal blood flow was achieved upon removing the clamps, and then, the incision was closed. The sham group were subjected to the same surgical procedure except for the fastening of the bilateral renal pedicles. All rats were then housed again with free access to food and water.

Ultrasound resolution microvascular imaging settings, data acquisition, and processing

Ultrasound resolution microvascular imaging was conducted 24 h post-reperfusion. Rats were anesthetized by 5% isoflurane in 65% nitrogen and 35% oxygen; 1–2% isoflurane maintained the anesthesia. Hemodynamic stability was ensured through: (1) standardized isoflurane anesthesia (1–2%) with respiratory monitoring and (2) core temperature maintenance at 37 °C using a heating pad. All ultrasound examinations were performed using a 5–15 MHz linear array probe (VINNO ULTIMUS 9E, China). B-mode imaging was used to optimize the imaging plane, making the maximum sagittal axis view of the

right kidney were represented. color Doppler flow imaging (CDFI) and superb microvascular imaging (SMI) were performed to assess renal blood flow. The contrast agent SonoVue® (Bracco, Milan, Italy), which consists of sulfur hexafluoride microbubbles was prepared according to the manufacturer's instructions. 0.045 ml/kg SonoVue® was diluted in 0.9% saline (1:1) and bolus injected through the tail vein, followed by a 0.5 mL flush of 0.9% saline. Data recording was initiated when contrast agent bolus injected, with ultrasound resolution microvascular imaging (mechanical index: 0.063, frame rate: 100–110 Hz) data being collected at 10-s intervals. A total of 12 video segments are amassed over a period of 3 min (Given that the post-acquisition storage process exceeds 10 s, the initiation of ultra-resolution imaging data collection is scheduled to commence every 15 s). All ultrasound acquisitions were performed handheld by an operator with > 5 years of experience, simulating clinical conditions. After respiratory stabilization under anesthesia, real-time quality control metrics provided by the VINNO system, such as interframe correlation and structural similarity, maintain the stability of the imaging plane. Inter-frame correlation analysis is carried out to filter out the motion data, and then fast and accurate motion compensation is carried out on the stationary data to reduce the influence of motion. To minimize errors, all the injections of contrast agent was undertaken by the same operator.

Ultrasound resolution microvascular imaging data processing workflow

The processing workflow comprised four key stages: (1) raw ultrasound signals were processed using a multi-stage filtering approach: first, singular value decomposition (SVD) with adaptive truncation thresholds suppressed tissue clutter; subsequently, temporal frequency-domain filtering isolated microbubble signatures. This dual-filtering strategy ensured robust microbubble detection across varying flow velocities by dynamically adjusting to signal characteristics while preserving microvascular flow information. (2) Sub-pixel localization: microbubble positions were resolved at sub-wavelength resolution via adaptive deconvolution and accelerated gradient-based localization. (3) Motion tracking and compensation: the accelerated Kalman pursuit method combined with probabilistic and linear motion model constraints is used to fast track the positioning point set, and the motion of microbubbles at different speeds can be well-captured in a very short time. (4) Microvascular mapping: accumulated microbubble trajectories generated density maps (vessel morphology) and velocity maps (directional flow).

We manually outlined the region of interest (ROI) in the kidney by a trackball-guided cursor technique. ROI was defined in the area of the subcapsular cortex. Video clips from URM were digitally stored for subsequent quantitative analysis with the built-in software URM QAT (URM Quantitative Analysis Toolkit). The images of density, direction and velocity map were obtained. The quantitative parameters including vascular density, complexity level, microvascular velocity, minimum diameter of vessel and perfusion index were measured within the selected ROI (Fig. 1, Table 1).

Blood biochemistry

After ultrasound examination, 2 mL blood was collected from the inferior vena cava. Standing for 1 h at room temperature, the supernatant was collected by centrifuged at 3000 r/min for 10 min and then frozen at −20 ℃. Serum levels of creatinine (Cr) and blood–urea–nitrogen (BUN) were measured with the biochemical analyzer Hitachi-8000 (Hitachi, Tokyo, Japan).

Histology and immunohistochemistry

The right kidney was harvested from each animal and weighted, then fixed in 10% formalin. The specimen was embedded in paraffin and cut into 3 μm sections. The sections were examined using periodic acid-Schiff (PAS) staining and the CD31 immunohistochemistry by two pathologists who were blinded to the study design.

The kidney tubular damage was categorized into six distinct levels [14]: Level 0 indicates no damage; Level 1 signifies mild injury, affecting 0–10% of the tubules; Level 2 denotes moderate damage, with 11–25% involvement; Level 3 is characterized by severe injury, involving 26–49% of the tubules; Level 4 represents highly severe injury, affecting 50–75%; and Level 5 corresponds to extensive damage, impacting over 75% of the kidney tubules. CD31 immunohistochemistry was employed as a quantitative measure of microvascular structural integrity and endothelial damage. For CD31 immunohistochemistry, images were photographed in a blinded fashion for each rat in the study. At least 5 low-power (10X) images were obtained. Quantitation was performed using the percent area function of Image J (NIH, Bethesda MD) using a common threshold for all images.

Statistical analysis

All data are expressed as mean ± standard deviation (SD). Data that were normally distributed, or that could be transformed to be normally distributed, were analyzed with a one-way ANOVA with post-hoc Tukey's test. Otherwise, the non-parametric Mann–Whitney *U* test was used. Associations between URM parameters and CD31/Cr/BUN were analyzed using Pearson or Spearman correlation depending on data normality. Inter-observer agreement was analyzed

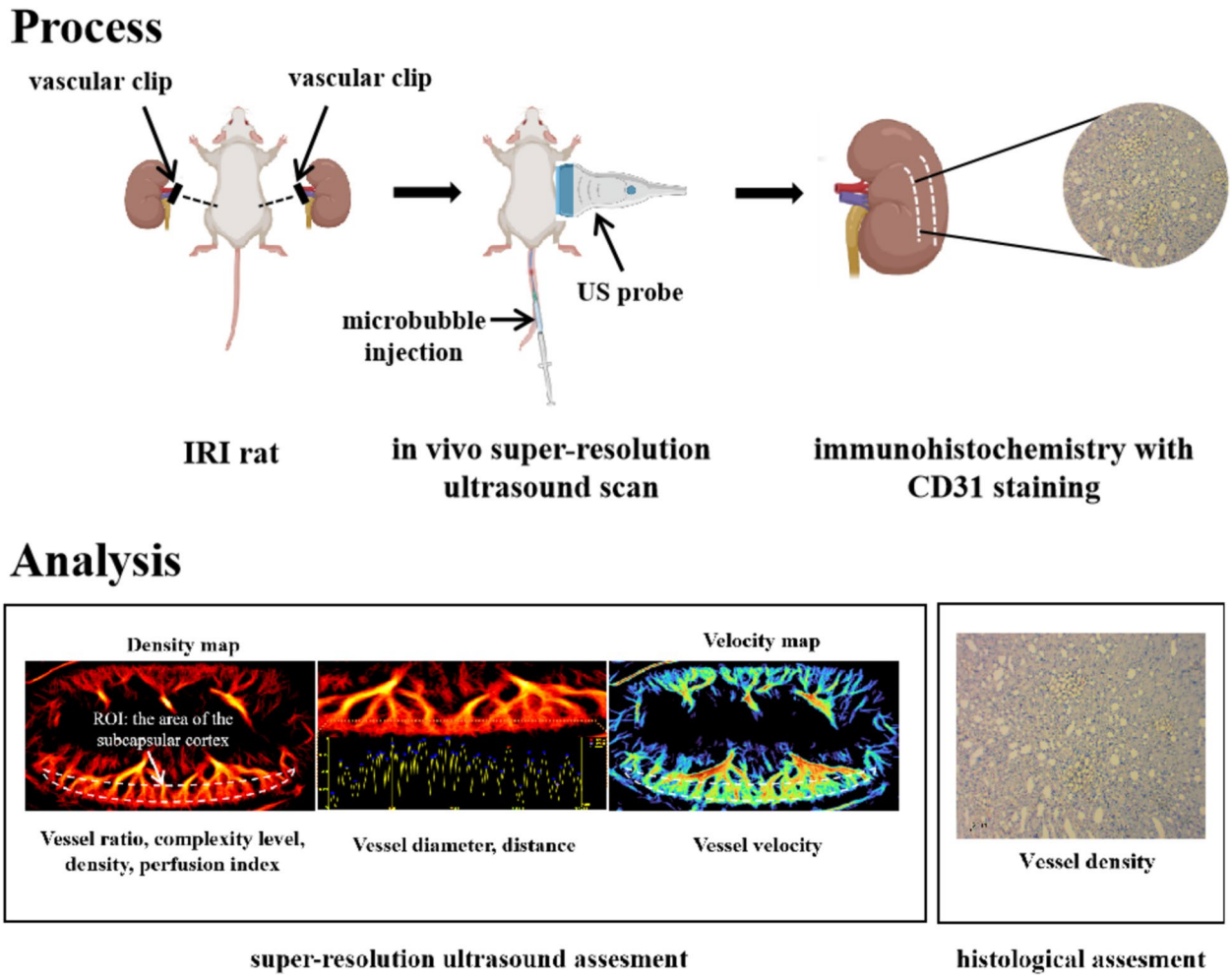

Fig. 1 Scheme of the experiment

Table 1 Microvascular parameters in the URM analysis

Parameter name	Unit	Definition
Vessel ratio	%	Area of vessel density area in the ROI/total area of the ROI
Complexity level	w.u	The degree of morphological, structural, and geometric confusion of the vascular system in the ROI
Mean density	a.u	Mean values of the vessel density regions in the ROI
Perfusion index	w.u	Mean vessel velocity in the ROI * proportion of vessel density in the ROI
Mean velocity	mm/s	Distance of intravascular fluid movement per unit of time
Min diameter	μm	Minimum diameter of each vessel within the span range of the sampling line

using Bland–Altman plot. Statistical analyses were performed using Prism 9.0 (GraphPad). The $p < 0.05$ was considered statistically significant.

Results

URM analysis time period

After URM performed, a total of 12 video segments were collected over a period of 3 min in every kidney. In addition, the quantitative parameters including vascular density, complexity level, microvascular velocity and perfusion index were measured in every segment. From Fig. 2A–E, it can be observed that the URM parameters during the 30 s–1 min time frame are more stable compared to other periods, and the Bland–Altman plot also indicates good inter-observer agreement. (Table 2, Fig. 2a–e) Therefore, in subsequent studies, we will adopt the 30 s–1 min time interval for analysis.

Comparison of URM with Doppler modes

Compared to CDFI and SMI (Fig. 3A, B) techniques, interlobar vessels, arcuate vessels, and cortical radial vessels were more visible in URM (Fig. 3C). In addition, the medullary organization was visible by the URM density map, whereas it is not with CDFI and SMI modes (Fig. 3). The average of the smallest vessel in the control group measured 0.11 ± 0.01 mm for URM, 0.50 ± 0.08mm for SMI, 0.80 ± 0.12mm for CDFI, that was, about 4 to 7 times thinner with URM than with other techniques.

URM density, directivity and velocity maps

Interlobar vessels, arcuate vessels and cortical radial vessels were visible on URM density maps (Fig. 4A). Medullary organization and smaller structures were not clearly detectable by clinical URM. URM directivity maps, that was, upward flows in red and downward flows in blue, highlighted cortical radial arteries and veins more precisely (Fig. 4B). The URM speed maps (Fig. 4C) indicated a decrease in velocity as the vessels approach the kidney capsule.

Quantitative density and speed analysis in the cortex area

Figure 4a–c shows the kidney cortical mean vessel ratio, mean density and perfusion index in the IRI group differed significantly from the control and sham group ($p < 0.0001, = 0.0237, = 0.0028$). The mean vessel ratio, mean density and perfusion index were 87.11 ± 4.31%, 12.61 ± 1.95, 12.74 ± 1.78 for control kidneys, 85.66 ± 3.05%, 12.55 ± 3.01, 11.89 ± 1.31 for sham, 43.27 ± 7.65%, 8.60 ± 2.53, 8.55 ± 2.25 for IRI kidneys. While there were no significant differences in complexity level and mean velocity among the three groups (Fig. 4d, e, $p > 0.05$).

Kidney function results

Compared to the control and sham group, serum levels of Cr and BUN were significantly increased in the experimental group ($p < 0.0001, = 0.0095$). There were no significant differences between the control and sham group ($p = 0.8043$, 0.9482) (Fig. 5A, B).

Figure 5C–H compares the kidney function with URM assessment of the vessel ratio, mean density and perfusion index. There were significant correlations between Cr and vessel ratio ($p = 0.0025$, $r = -0.67$), mean density ($p = 0.0009$, $r = -0.71$), perfusion index ($p = 0.0004$, $r = -0.75$). Meanwhile, BUN were inversely correlated with vessel ratio ($p = 0.0083$, $r = -0.60$), mean density ($p = 0.0122$, $r = -0.58$), perfusion index ($p = 0.0006$, $r = -0.73$).

Kidney histology and immunohistochemistry results

There was no obvious change of kidney glomerulus and tubule in the control and sham group. Glomerular structure in the IRI group was also not significantly changed. The kidney tubular injury in the IRI group was predominantly localized to the distal convoluted tubules, where detachment of the brush border, flattened epithelial cells, deposition of cellular debris and formation of tubular cast were evident (6A–C). The result of kidney tubular injury score showed that the score of the IRI group was significantly higher than those of the control and sham group, with statistical significance ($p < 0.0001$) (Fig. 6D).

Figure 7A–C shows CD31 Immunohistochemistry of the control, sham, and IRI kidneys. The mean vessel density in the kidney from each group determined as the fractional area of staining from a midsagittal slice of the kidney, was 0.081 ± 0.022 for control kidneys, 0.077 ± 0.018 for sham, 0.044 ± 0.012 for IRI kidneys (Fig. 7D). Figure 7E–G compares the histology with URM assessment of the vessel ratio, mean density and perfusion index. There were significant correlations between CD31 and vessel ratio ($p = 0.0018$, $r = 0.68$), mean density ($p = 0.0043$, $r = 0.64$), perfusion index ($p = 0.0060$, $r = 0.62$), supporting the accuracy of the microvascular assessment by URM imaging.

Discussion

This study showed the feasibility of URM in acute kidney injury induced by IRI using a conventional clinical ultrasound scanner. We demonstrated that with very simple examination procedure and post-processing tools, we were able to improve the resolution of kidney

microvascular imaging. URM density and directivity maps revealed the different kidney structures and that URM maps reached 4–7 times thinner vessel diameter than the conventional CDFI and SMI modes. Furthermore, velocities in cortical regions depend on their distance from the kidney capsule.

This study used bilateral IRI to induce the classic model of AKI in rats [15]. The operation is simple and the effect is relatively stable. The diagnosis of AKI was based on an increasing serum Cr [16] and kidney pathology. The results exhibited URM imaging was sensitive enough to detect changes in kidney microvasculature with quantitative analysis. The changes in kidney microvascular density and velocity were successfully quantified from high quality URM images and demonstrated kidney function biochemical parameters and pathologic changes in IRI rats. The close correlation ($r=0.62–0.68$) between the

Table 2 Bland–Altman plot analysis obtained by observers 1 and 2

Observer	Mean ± SD	95% CI	95% LOA
Vessel ratio	2.433 ± 4.017	−0.120 to 4.985	−10.31 to 5.441
Complexity level	−0.017 ± 0.086	−0.071 to 0.038	−0.152 to 0.185
Mean density	0.029 ± 2.329	−1.451 to 1.509	−4.594 to 4.536
Perfusion Index	0.602 ± 1.409	−0.294 to 1.497	−3.363 to 2.160
Mean velocity	−0.324 ± 2.718	−2.051 to 1.402	−5.002 to 5.651

Mean Mean of differences (observer 2-1), *SD* SD of differences, *95% CI* 95% Confidence Internal, *95% LOA* 95% Limits of Agreement

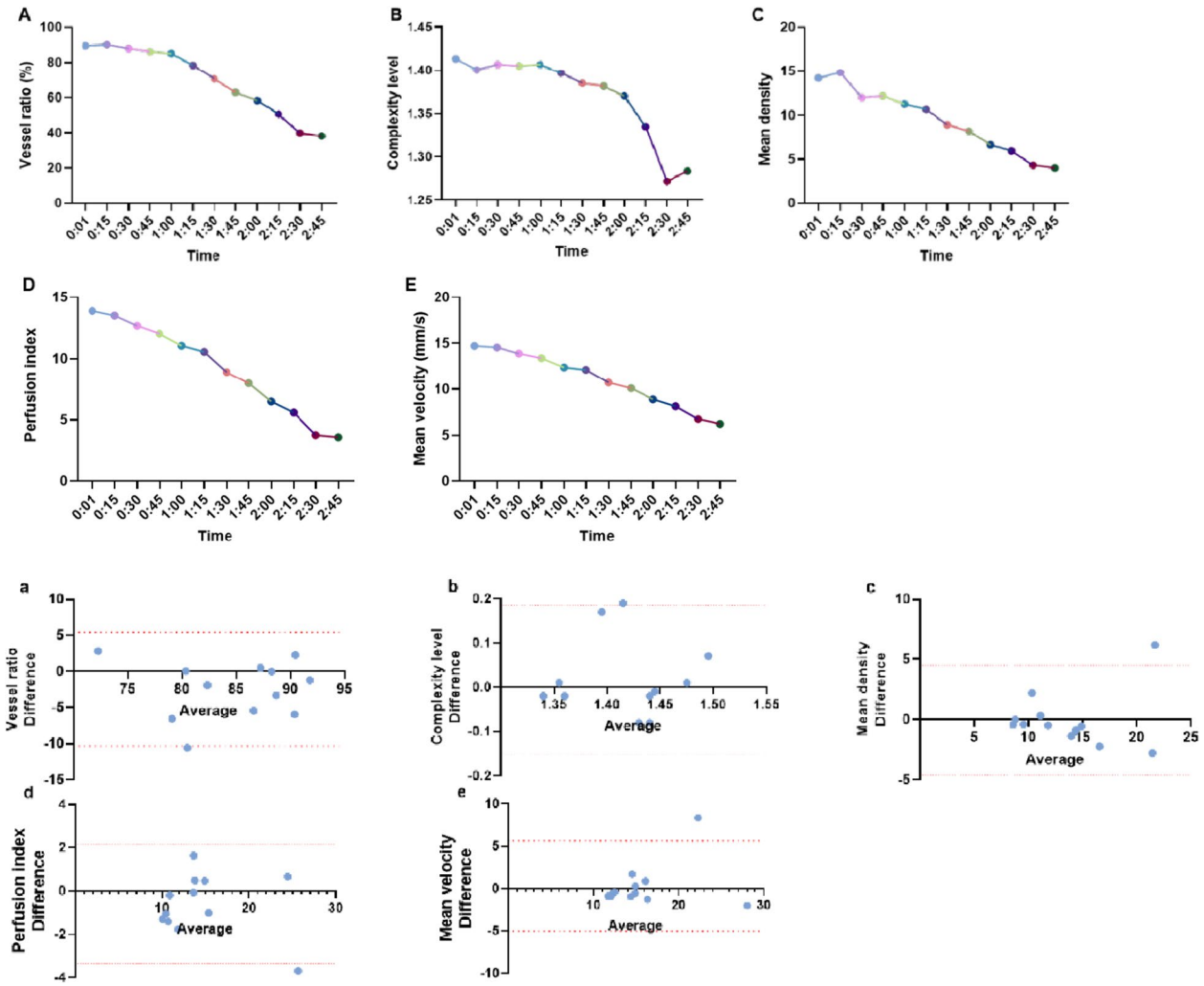

Fig. 2 Trends of URM parameters during the 1 s–3 min time and inter-observer agreement of URM parameters. **A**–**E** Time-course analysis (1 s–3 min) of **A** vessel ratio, **B** complexity level, **C** mean density, **D** perfusion index and **E** mean velocity. **a**–**e** Inter-observer agreement was performed for the **a** vessel ratio, **b** complexity level, **c** mean density, **d** perfusion index and **e** mean velocity. *URM* ultrasound resolution microvascular imaging

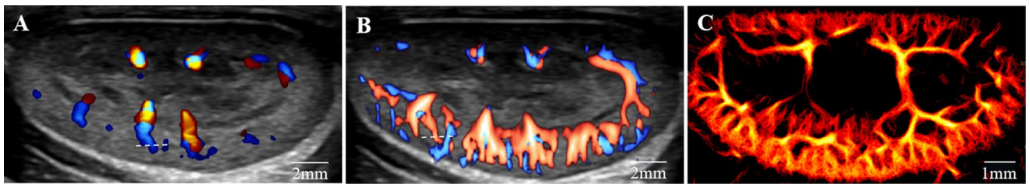

Fig. 3 Smallest imageable vessel diameter measured in ultrasound resolution microvascular imaging (URM) and in Doppler classical modes in control group. **a** Color Doppler. **b** Super microvascular imaging (SMI). **c** URM. The white dotted center marks indicate the smallest imageable blood vessel

URM and histology validated the feasibility and accuracy of URM for kidney vasculature assessment.

The degree of microvascular reconstruction in super-resolution imaging depends on the observation time, flow rate, and contrast agent concentration [17, 18]. Previous literature indicates that the measurement time varies from a few seconds to several minutes [19, 20], leading to differences in the number of resolved microvessels

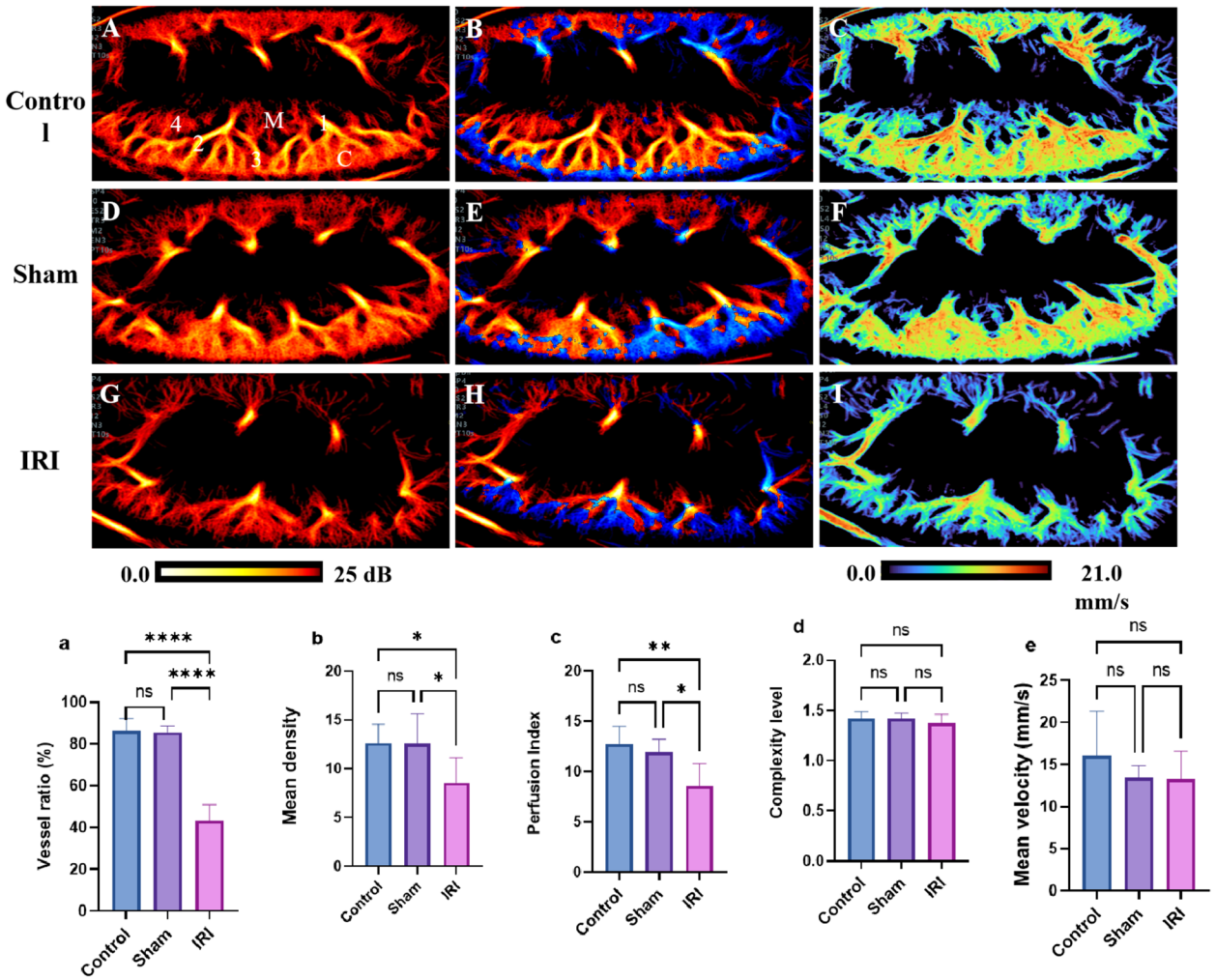

Fig. 4 Ultrasound resolution microvascular imaging (URM) density, directivity and speed maps. **A**–**C** URM density (**A**), directivity (**B**) and speed (**C**) maps in control group. C is for kidney cortex, M for medullary organization, 1 for interlobar vessels, 2 for arcuate vessels, 3 for interlobular vessels (cortical radial vessels), and 4 for vasa recta. **D**–**F** URM density (**A**), directivity (**B**) and speed (**C**) maps in sham group. **G**–**I** URM density (**A**), directivity (**B**) and speed (**C**) maps in IRI group. **a**–**e** Quantitative analysis of URM between control, sham and IRI group. **a** Vessel ratio, **b** mean density, **c** perfusion index, **d** complexity level and **e** mean velocity. IRI: ischemia–reperfusion injury. *$p < 0.05$, **$p < 0.01$, ****$p < 0.0001$

[18]. Therefore, it is necessary to standardize the measurements to derive reproducible quantitative parameters from URM. URM imaging is based on the central localization of sparse single microbubbles, achieving super-resolution structural reconstruction through the frame-by-frame accumulation of localization events [19]. To ensure the accuracy of microbubble localization, it is essential that the spatial distribution of microbubbles is sparse and that the microbubbles undergo positional changes over time, allowing for the accumulation of different localization events in both space and time. Hence, the speed of blood flow and the concentration of injected microbubbles are crucial for image quality. Our research group previously explored the concentration and ultimately determined the optimal concentration for super-resolution imaging.

During URM imaging process, it is unknown whether the URM data collected at different timepoints can accurately reflect the true microcirculatory perfusion status of the kidney as the contrast agent fades. Therefore, to ensure the consistency of the analysis results, data recording begins at the time of the bolus injection of the contrast agent (0s), with a collection time of 10 s, and a total of 12 video clips are collected within 3 min (since the URM data storage process exceeds 10 s, the URM data collection is initiated every 15 s). Subsequently, by comparing the URM images and quantitative parameter results of rats in the normal group at different timepoints, we identified the timepoints (30–60 s) that best represent the kidney perfusion status. These timepoints are used for subsequent analysis of the microvascular state of the rat kidneys to ensure the accuracy and reliability of the research results. To minimize the impact of the contrast agent bolus injection speed, all injection operations are performed by the same researcher.

URM for imaging kidney microvascular changes has been studied before in rat IRI model [21]. However, this study was performed on limited animal samples and without quantification parameters and statistical support. In this study, we used increased number of animals and groups to determine statistical significance. We have also assessed the kidney microvascular changes with quantification parameters. This study demonstrates that URM quantitatively detects microvascular rarefaction and perfusion deficits in IRI–AKI, consistent with established pathophysiology. Ischemia–reperfusion injury triggers endothelial cell dysfunction, characterized by nitric oxide (NO) depletion, increased vasoconstrictors (e.g., endothelin-1), and inflammatory activation [22, 23]. This cascade promotes microvascular congestion, vasoconstriction, and capillary dropout—key hallmarks of AKI [2, 3]. URM is uniquely positioned to capture these alterations: its superior spatial resolution (0.11 mm) enables the visualization of critical microvascular structures, such as arcuate vessels, which remain invisible to conventional Doppler and SMI techniques

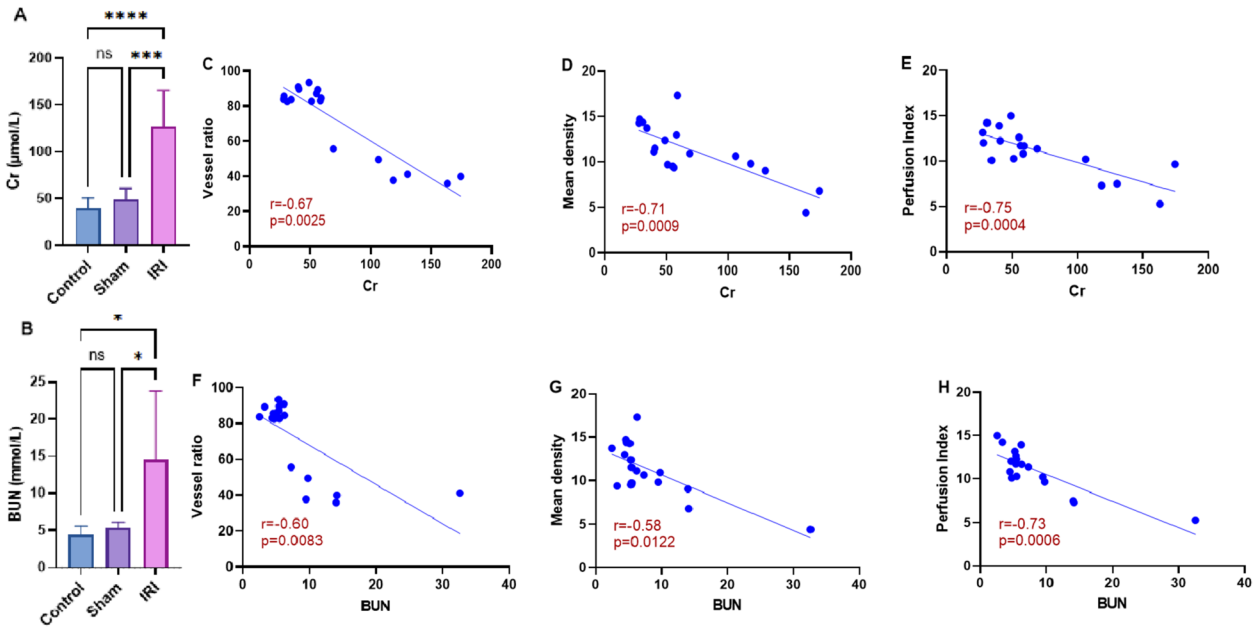

Fig. 5 Kidney function biomarkers and correlation with URM imaging. **A**, **B** Comparison of the serum Cr and BUN levels. **C**–**E** Significant correlation between Cr and vessel ratio, mean density and perfusion index. **F**–**H** Significant correlation between BUN and vessel ratio, mean density and perfusion index. *Cr* creatinine, *BUN* blood–urea–nitrogen, *URM* ultrasound resolution microvascular imaging, *IRI* ischemia–reperfusion injury. *$p < 0.05$, ****$p < 0.0001$

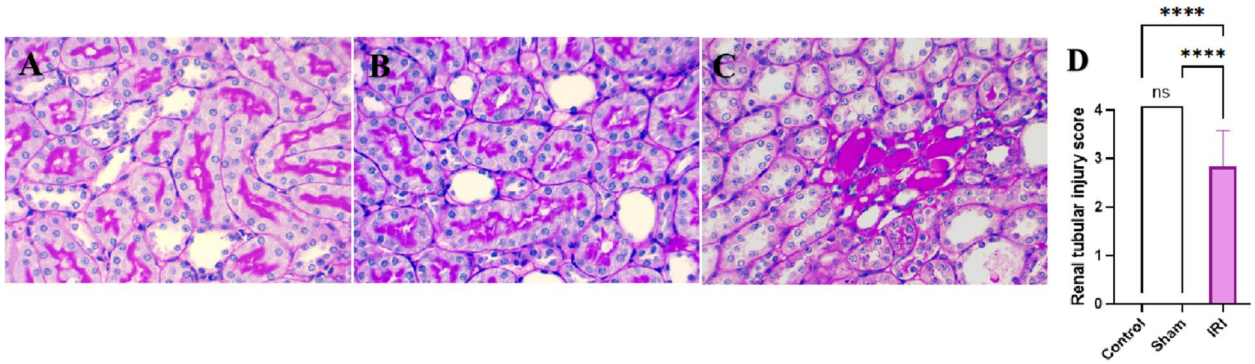

Fig. 6 Kidney tubular pathological changes (PAS, ×40). **A**–**C** Representative histopathologic images of the kidney using PAS staining (**A** control, **B** sham, **C** IRI). **D** Comparison of kidney tubular injury score. *URM* ultrasound resolution microvascular imaging, *IRI* ischemia–reperfusion injury. ****$p < 0.0001$

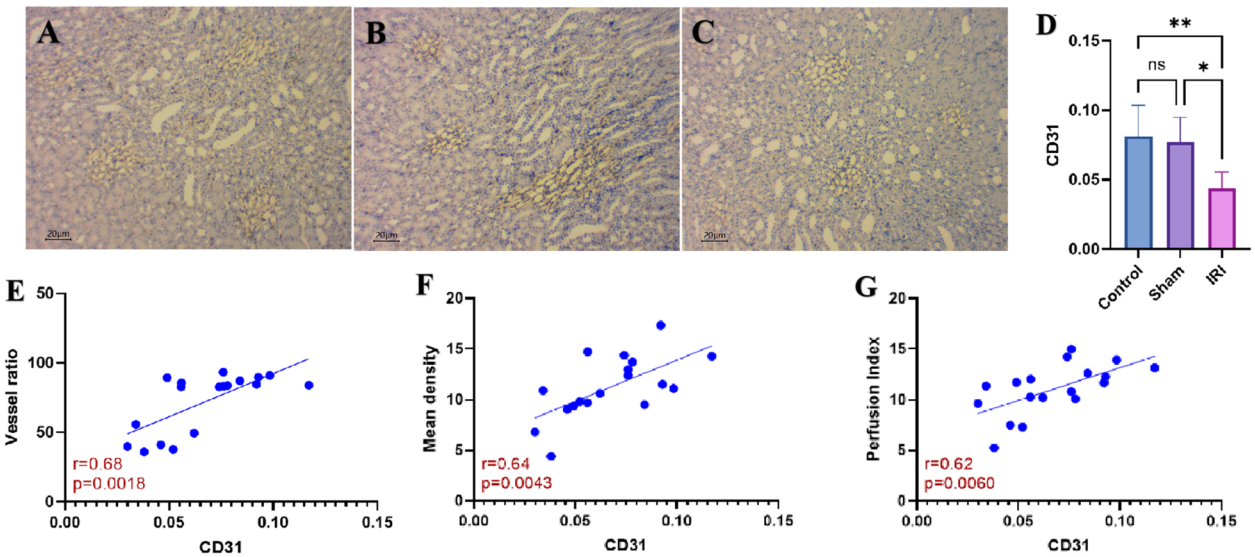

Fig. 7 Vessel density by CD31 immunohistochemistry and correlation with URM imaging. **A**–**C** Representative CD31 staining of the control, sham, and IRI kidneys. **D** Comparison of vessel density measured by CD31 immunohistochemistry. **E**–**G** Significant correlation between the histology measurement of the vessel density and URM parameters of vessel ratio, mean density and perfusion index were found. *URM* ultrasound resolution microvascular imaging, *IRI* ischemia–reperfusion injury. *$p < 0.05$, **$p < 0.01$

(limited to 0.5–0.8 mm), thereby directly quantifying capillary loss. Furthermore, the derived perfusion index reflects the resulting hemodynamic impairment stemming from endothelial dysfunction and vasoconstriction, evidenced by its strong inverse correlation with serum Cr and BUN levels ($r = -0.58$ to 0.75). Complementing this, the measured vessel density shows a significant positive correlation with the reduction in $CD31^+$ area ($r = 0.62$–0.68), confirming URM's ability to noninvasively map the structural rarefaction of the microvasculature. Importantly, CD31 is not only a structural marker of endothelial cells but its reduced expression is a recognized indicator of endothelial dysfunction and activation in AKI [11]. The strong correlation between URM vessel density and $CD31^+$ area reduction thus provides indirect validation that URM detects microvascular changes driven by endothelial injury. Thus, URM transcends traditional ultrasound by detecting early microcirculatory failure and structural rarefaction—critical for AKI diagnosis prior to functional decline. While this study did not directly assess soluble markers of endothelial dysfunction (e.g., circulating endothelin-1 and ICAM-1), our URM parameters (perfusion index, vessel density) and their correlations with CD31 immunohistochemistry and renal function strongly support the role of endothelial injury in the observed microvascular alterations. Future

studies incorporating direct measurement of endothelial dysfunction markers alongside URM could provide even deeper mechanistic insights into the temporal relationship between endothelial activation, microvascular hemodynamic changes, and structural rarefaction in AKI.

Nevertheless, this study has some limitations. First, conventional Doppler imaging, SMI and URM are not precisely aligned in the same plane, as the probe is handheld and the examinations are conducted minutes apart. Consequently, quantitative estimations derived from these methods are subject to bias and should be regarded as indicative rather than definitive. Second, we standardized anesthesia to minimize hemodynamic variation, future studies will incorporate non-invasive blood pressure monitoring. Nevertheless, the absence of microvascular changes in sham-operated controls under identical conditions supports that observed alterations in IRI rats reflect intrinsic renal pathology rather than systemic confounders. Third, while URM achieved 0.11 mm resolution in rats using a high-frequency linear probe (5–15 MHz), clinical abdominal probes (typically 2–5 MHz) may yield lower resolution due to greater tissue penetration depths and larger footprints. Future human studies should optimize microbubble infusion protocols, develop motion compensation algorithms, and validate acquisition times for abdominal applications. Finally, since CEUS is a much simpler and faster technology than URM, can URM provide better quantitative results than CEUS, thereby leading to more accurate diagnoses? In the future, we need to conduct relevant preclinical and clinical comparative studies.

Conclusion

This study demonstrated that detailed ultrasound super-resolution images of the kidney vasculature of rat kidneys are obtainable with clinical ultrasound equipment. URM imaging provides promising method for noninvasive visualization and quantification of vessel characteristics. Future studies will aim at investigating dynamic changes at 6 h, 24 h and 72 h to map temporal progression of microvascular alterations.

Abbreviations

AKI	Acute kidney injury
BUN	Bloodureanitrogen
CDFI	Color Doppler flow imaging
CEUS	Contrast-enhanced ultrasound
Cr	Creatinine
IRI	Ischemia reperfusion injury
IRI–AKI	Ischemia–reperfusion-induced acute kidney injury
Micro-CT	Micro-computed tomography
MRI	Magnetic resonance imaging
ROI	Region of interest
SMI	Superb microvascular imaging
URM	Ultrasound resolution microvascular

Acknowledgements
The authors thank Vinno Technology (Suzhou) Co., Ltd, China for providing guidance on ultrasound resolution microvascular imaging.

Author contributions
Ping Zhao designed the study, conducted the study, acquired and analyzed the data and wrote the manuscript. Jianing Zhu acquired and analyzed the data and revised the manuscript. Huina An and Luda Song analyzed data and revised the manuscript. Yiru Wang and Qiuyang Li revised the manuscript. Yukun Luo designed the study and revised the manuscript. All authors read and approved the final manuscript.

Funding
This research was supported by the National Natural Science Foundation of China (No.82371985) and Beijing Natural Science Foundation (No.7232352).

Data availability
No datasets were generated or analysed during the current study.

Declarations

Ethics approval and consent to participate
The study protocol was approved by the Ethics Committee of the PLA General Hospital (2023-X19-45).

Consent for publication
Not applicable.

Competing interests
The authors declare no competing interests.

Author details
[1]School of Medicine, Nankai University, Tianjin 300071, China. [2]Department of Ultrasound, First Medical Center, Chinese PLA General Hospital, Beijing 100853, China. [3]Department of Nephrology, First Medical Center of ChineseState Key Laboratory of Kidney DiseasesBeijing Key Laboratory of Kidney Disease Research, PLA General Hospital, Nephrology Institute of the Chinese People's Liberation Army, National Clinical Research Center for Kidney Diseases, Beijing 100853, China.

Received: 17 February 2025 Accepted: 26 September 2025
Published online: 12 November 2025

References

1. Mercado MG, Smith DK, Guard EL. Acute kidney injury: diagnosis and management. Am Fam Physician. 2019;100(11):687–94.
2. Zafrani L, Ince C. Microcirculation in acute and chronic kidney diseases. Am J Kidney Dis. 2015;66(6):1083–94.
3. Sutton TA. Alteration of microvascular permeability in acute kidney injury. Microvasc Res. 2009;77(1):4–7.
4. Ehling J, Babickova J, Gremse F, Klinkhammer BM, Baetke S, Knuechel R, et al. Quantitative micro-computed tomography imaging of vascular dysfunction in progressive kidney diseases. J Am Soc Nephrol. 2016;27(2):520–32.
5. Prowle JR, Molan MP, Hornsey E, Bellomo R. Measurement of renal blood flow by phase-contrast magnetic resonance imaging during septic acute kidney injury: a pilot investigation. Crit Care Med. 2012;40(6):1768–76.
6. Xu Z, Zhao X, Huang M, Liu Q, Liu L, Zheng J, et al. Evaluation of renal ischemia-reperfusion injury using CEUS in mice. Eur Radiol Exp. 2023;7(1):81.
7. Wang X, Chen L, Su T. Evaluating renal microcirculation in patients with acute kidney injury by contrast-enhanced ultrasonography: a protocol for an observational cohort study. BMC Nephrol. 2022;23(1):392.
8. Watchorn J, Huang D, Bramham K, Hutchings S. Decreased renal cortical perfusion, independent of changes in renal blood flow and sublingual microcirculatory impairment, is associated with the severity of acute kidney injury in patients with septic shock. Crit Care. 2022;26(1):261.

9. Song P, Rubin JM, Lowerison MR. Super-resolution ultrasound microvascular imaging: is it ready for clinical use? Z Med Phys. 2023;33(3):309–23.
10. Demeulenaere O, Bertolo A, Pezet S, Ialy-Radio N, Osmanski B, Papadacci C, et al. In vivo whole brain microvascular imaging in mice using transcranial 3D ultrasound localization microscopy. EBioMedicine. 2022;79:103995.
11. Chen Q, Yu J, Rush BM, Stocker SD, Tan RJ, Kim K. Ultrasound super-resolution imaging provides a noninvasive assessment of renal microvasculature changes during mouse acute kidney injury. Kidney Int. 2020;98(2):355–65.
12. Huang C, Zhang W, Gong P, Lok UW, Tang S, Yin T, et al. Super-resolution ultrasound localization microscopy based on a high frame-rate clinical ultrasound scanner: an in-human feasibility study. Phys Med Biol. 2021;66(8):08NT01.
13. Demene C, Robin J, Dizeux A, Heiles B, Pernot M, Tanter M, et al. Transcranial ultrafast ultrasound localization microscopy of brain vasculature in patients. Nat Biomed Eng. 2021;5(3):219–28.
14. Yang B, Lan S, Dieude M, Sabo-Vatasescu JP, Karakeussian-Rimbaud A, Turgeon J, et al. Caspase-3 is a pivotal regulator of microvascular rarefaction and renal fibrosis after ischemia-reperfusion injury. J Am Soc Nephrol. 2018;29(7):1900–16.
15. Singh AP, Junemann A, Muthuraman A, Jaggi AS, Singh N, Grover K, et al. Animal models of acute renal failure. Pharmacol Rep. 2012;64(1):31–44.
16. Ostermann M, Bellomo R, Burdmann EA, Doi K, Endre ZH, Goldstein SL, et al. Controversies in acute kidney injury: conclusions from a Kidney Disease: Improving Global Outcomes (KDIGO) conference. Kidney Int. 2020;98(2):294–309.
17. Dencks S, Piepenbrock M, Opacic T, Krauspe B, Stickeler E, Kiessling F, et al. Clinical pilot application of super-resolution US imaging in breast cancer. IEEE Trans Ultrason Ferroelectr Freq Control. 2019;66(3):517–26.
18. Dencks S, Piepenbrock M, Schmitz G. Assessing vessel reconstruction in ultrasound localization microscopy by maximum likelihood estimation of a zero-inflated Poisson model. IEEE Trans Ultrason Ferroelectr Freq Control. 2020;67(8):1603–12.
19. Christensen-Jeffries K, Couture O, Dayton PA, Eldar YC, Hynynen K, Kiessling F, et al. Super-resolution ultrasound imaging. Ultrasound Med Biol. 2020;46(4):865–91.
20. Dencks S, Schmitz G. Ultrasound localization microscopy. Z Med Phys. 2023;33(3):292–308.
21. Andersen SB, Taghavi I, Hoyos CAV, Sogaard SB, Gran F, Lonn L, et al. Super-resolution imaging with ultrasound for visualization of the renal microvasculature in rats before and after renal ischemia: a pilot study. Diagnostics. 2020;10(11):862.
22. Krishnan S, Suarez-Martinez AD, Bagher P, Gonzalez A, Liu R, Murfee WL, et al. Microvascular dysfunction and kidney disease: challenges and opportunities? Microcirculation. 2021;28(3):e12661.
23. Huang MJ, Ji YW, Chen JW, Li D, Zhou T, Qi P, et al. Targeted VEGFA therapy in regulating early acute kidney injury and late fibrosis. Acta Pharmacol Sin. 2023;44(9):1815–25.

Publisher's Note